Contrast gain control and cortical TrkB signaling shape visual acuity

J Alexander Heimel, M Hadi Saiepour, Sridhara Chakravarthy, Josephine M Hermans, Christiaan N Levelt

▶ **To cite this version:**

J Alexander Heimel, M Hadi Saiepour, Sridhara Chakravarthy, Josephine M Hermans, Christiaan N Levelt. Contrast gain control and cortical TrkB signaling shape visual acuity. Nature Neuroscience, 2010, 10.1038/nn.2534 . hal-00527058

HAL Id: hal-00527058
https://hal.science/hal-00527058

Submitted on 18 Oct 2010

HAL is a multi-disciplinary open access archive for the deposit and dissemination of scientific research documents, whether they are published or not. The documents may come from teaching and research institutions in France or abroad, or from public or private research centers.

L'archive ouverte pluridisciplinaire **HAL**, est destinée au dépôt et à la diffusion de documents scientifiques de niveau recherche, publiés ou non, émanant des établissements d'enseignement et de recherche français ou étrangers, des laboratoires publics ou privés.

Contrast gain control and cortical TrkB signaling shape visual acuity

J. Alexander Heimel, M. Hadi Saiepour, Sridhara Chakravarthy, Josephine M. Hermans & Christiaan N. Levelt

Molecular Visual Plasticity Group, Netherlands Institute for Neuroscience, an institute of the Royal Netherlands Academy of Arts and Sciences, Meibergdreef 47, 1105 BA Amsterdam, The Netherlands. Correspondence should be addressed to J.A.H. (heimel@nin.knaw.nl)

During development, aging and in amblyopia, visual acuity is much below the limitations set by the retina. Expression of brain-derived neurotrophic factor (BDNF) in the visual cortex is reduced in these situations. We have tested the hypothesis that TrkB/BDNF regulates cortical visual acuity in adult mice. We found that genetically interfering with TrkB/BDNF signaling in pyramidal cells in the mature visual cortex reduced synaptic strength and resulted in a loss of neural responses to high spatial frequency stimuli. Responses to low spatial frequency stimuli were unaffected. This selective loss was not accompanied by a change in receptive field sizes or plasticity but exclusively by a reduction in apparent contrast. We demonstrate that a dependence on spatial frequency in the Heeger normalization model explains this selective effect of contrast reduction on high resolution vision, and argue that it involves contrast gain control operating within the visual cortex.

Resubmission date: March 5th, 2010

The limits of visual acuity and contrast sensitivity are set by the eye, but what we perceive is determined by the visual cortex[1]. In healthy, mature people and animals, the visual acuities of the retina and the cortex are well-matched[2], but this match is neither automatic nor unbreakable. Differences between cortical and retinal acuity are most apparent during development, when cortical acuity continues to rise after retinal development is completed[3], and during aging, when behavioral acuity falls even without obvious changes in the eye or the thalamus[4]. Differences also occur as a result of cortical injury or erroneous development. This is the case with amblyopia, the most prevalent (2-4%) visual impairment in young people. Amblyopia is a reduced psychophysical acuity in one or both eyes. It is believed to be caused by deficient processing in the visual cortex[5], but the mechanisms underlying the dissociations of retinal and cortical acuity in amblyopia and in the healthy aging and developing brain are unclear. Interestingly, there is a good match between changes in the cortical expression level of brain-derived neurotrophic factor (BDNF) and changes in visual acuity. During development, acuity and BDNF levels rise[6], while both slowly decrease with age[4,7] . This relationship between BDNF and acuity also holds for experimentally induced amblyopia. BDNF mRNA and protein levels[8,9] and acuity[10] in the primary visual cortex (V1) responding to a monocularly deprived eye are all below normal. In amblyopic rats receiving environmental enrichment[11] or antidepressant treatment[12], increased BDNF expression in the cortex was seen in parallel to the restoration of visual acuity. Moreover, transgenic mice overexpressing BDNF in the forebrain show a faster rise of cortical acuity[6] even when reared in darkness[13]. Although there is a wealth of data on the involvement of BDNF and its main receptor TrkB in neuronal development[14], synaptic efficacy[15], -morphology[16] and -plasticity[17,18], it has remained unknown how BDNF promotes visual acuity at the coding level and whether BDNF signaling plays a role in acuity in the mature cortex. For these reasons we studied visual acuity in adult transgenic mice where, after normal development is completed, cortical TrkB/BDNF signaling is impaired. We found a loss of acuity, caused by a reduction in apparent contrast. Using a combination of experiments and modeling, we show the involvement of cortical gain control in the selective loss of responses to visual stimuli with high spatial frequencies and the maintenance of responses to low spatial frequencies.

RESULTS

Genetic inhibition of TrkB signaling in the adult cortex

To investigate the role of TrkB signaling in cortical acuity in the mature animal we overexpressed a dominant negative TrkB.T1-EGFP fusion protein[19] in a large proportion of pyramidal cells after the maturation of cortical acuity. This was achieved by crossing mice carrying a Cre-dependent *TrkB.T1-EGFP*-transgene under the control of the Thy-1 promoter[16] with *G35-3* Cre-recombinase transgenic animals[20] **(Supplementary Fig. 1)**. In *G35-3-Cre* mice, Cre-

recombination is restricted to excitatory neurons in the neocortex, hippocampus and amygdala[20] while the retina[21], thalamus and superior colliculus are unaffected. In *TrkB.T1-EGFP* x *G35-3* double transgenic animals, TrkB.T1-EGFP was expressed in excitatory neurons of the hippocampus and pyramidal neurons of the neocortex (**Fig. 1a**). Expression was absent in layer 4 of the neocortex (**Fig. 1b**), probably due to the lack of Thy-1 promoter activity in this layer. No transgene expression was detected in the locus coeruleus or basal forebrain neuromodulatory regions. Transgene expression started around 5 weeks after birth, after the end of the critical period for ocular dominance plasticity[22] and after maturation of visual acuity[6,10].

Synaptic efficacy is reduced by overexpression of TrkB.T1

Before investigating the effects of impaired TrkB signaling on visual processing in vivo, we assessed its effects at the synapse level. BDNF signaling is known to modulate synaptic transmission[15,18], and overexpression of TrkB.T1 inhibits BDNF-induced enhancement of excitatory transmission[23]. We therefore wanted to know whether interfering with TrkB signaling in pyramidal neurons of adult V1 altered synaptic transmission. We measured the response of pyramidal cells to electrical stimulation in slices of adult visual cortex of wild-type and TrkB.T1-EGFP-expressing mice. Because there was no expression of the transgene in layer 4 and TrkB/BDNF signaling has been implicated in both pre- and postsynaptic modulation of synaptic strength, we first studied the intralaminar connections of layer 2/3 to layer 2/3 neurons, which are the most abundant synapses in layer 2/3[24]. We recorded intracellular responses in layer 2/3 pyramidal neurons to extracellular stimulation by an electrode displaced 200 μm horizontally from the recording electrode in the same layer (**Fig. 1c-d**). These evoked responses were lower in TrkB.T1-EGFP-expressing animals than in wild-type mice (response to 200 μA, T1: 0.97±0.07 nA, 13 cells; wt: 1.9±0.2 nA, 6 cells; p=0.003, t-test, **Fig. 1e**) confirming a reduction in synaptic strength. Spike initiation thresholds were not different (T1: −35.1±0.9 mV; wt: −34.2±0.5 mV; p=0.5, t-test) nor was paired-pulse facilitation, a predominantly presynaptic phenomenon (T1: 1.18± 0.04; wt: 1.19± 0.03; p=0.9, t-test). Although the unchanged paired-pulse ratio did not fully exclude a presynaptic cause of the reduced synaptic strength, it did suggest a primarily post-synaptic phenotype. If so, we would expect a change in layer 4 to 2/3 connections as well. Therefore, we also recorded the local field potential (LFP) in layer 2/3 in response to extracellular stimulation by an electrode positioned in layer 4 (**Fig. 1f-g**). Evoked LFP responses are an indication of combined synaptic activity in the recording electrode's vicinity. In TrkB.T1-EGFP-expressing animals, responses were well below those in wild-type mice (response to 260 μA, T1: 1.50±0.14 mV, 14 slices, 6 mice; wt: 1.93±0.12 mV, 12 slices, 5 mice; p=0.03, t-test, **Fig. 1h**). The paired-pulse ratio was again unchanged (T1: 0.89±0.04; wt: 0.98±0.09; p=0.33, t-test). Together these results strongly suggest that in the TrkB.T1-EGFP expressing mice, synaptic transmission

to layer 2/3 neurons was reduced through a postsynaptic mechanism.

Evoked LFPs are dominated by excitatory synaptic transmission, but contain the combination of excitatory and inhibitory post-synaptic potentials. As chronic changes in BDNF signaling have been shown to positively correlate with the amount of perisomatic inhibition[6,25] by parvalbumin-expressing interneurons we also determined whether the *TrkB.T1-EGFP* transgenic animals showed changes in inhibitory inputs using immunohistochemistry. We examined the parvalbumin-positive boutons around pyramidal cell bodies, which provide the major source of inhibition in the cortex. This revealed that perisomatic inhibitory synapses were decreased in *TrkB.T1-EGFP* animals **(Supplementary Fig. 2)**, because both bouton number (T1: 2707 puncta in 418 cells, 3 mice; wt: 9048 puncta in 874 cells, 3 mice; $p<0.001$, t-test) and average bouton diameter were reduced (T1: 0.623±0.008 μm; wt: 0.715±0.005 μm; $p<0.001$, t-test). This finding suggests that the observed decrease in the evoked responses in layer 2/3 neurons was caused by an even larger decrease in excitatory transmission which was partially compensated for by reduced inhibitory input.

Acuity loss after inhibition of TrkB signaling

We next addressed the question whether the changes in synaptic transmission in adult TrkB.T1-EGFP-expressing mice were accompanied by a reduction in visual acuity by using optical imaging of intrinsic signal. Example responses to high contrast phase-reversing sinusoidal gratings of a wild-type mouse are shown in **Figures 2a-b**. Acuity was defined as the null response point of a threshold-linear curve fitted to the data (**Fig. 2b**). TrkB.T1-EGFP-expressing mice had a strongly reduced acuity (T1: 0.40±0.05 cycles per degree, N=7; wt: 0.54±0.03 cpd, N=18; $p=0.01$, t-test, **Fig. 2c**).

Closer inspection of the average response curves in **Figure 2d** shows that responses to the lowest tested spatial frequency (0.1 cpd) were not reduced ($p=0.6$, t-test). Because during development, increasing BDNF levels not only induce the increase in visual acuity but also the onset of the critical period[6], we tested the possibility that TrkB.T1-EGFP expression in the adult visual cortex would affect ocular dominance plasticity. However, no difference in ocular dominance plasticity was observed between wild-type and TrkB.T1-EGFP-expressing mice (**Supplementary Fig. 3**).

Acuity loss is caused by a reduction of apparent contrast

There are three functional mechanisms through which the excitatory and inhibitory synaptic changes could cause reduced acuity, illustrated in **Supplementary Figure 4**. The first mechanism is the enlargement of receptive field centers of neurons in the visual cortex. Sampling input from a larger retinal area would reduce the response to a high spatial frequency grating, because both dark and light areas will fall within single ON-/OFF-subfields of a neuron. The

second mechanism is a reduction of the signal-to-noise ratio (SNR) which may occur due to the reduction of inhibition and excitation. A reduced SNR would affect signal processing of high spatial frequency information more than of a low spatial frequency, because the response and therefore the SNR at high spatial frequencies is already smaller. The third mechanism is a reduction in perceived contrast. A reduction in synaptic transmission in TrkB.T1-EGFP-expressing mice would reduce the response to visual stimulation, as would a reduction of stimulus contrast. This abates the visibility of high spatial frequency stimuli more than that of lower spatial frequency, because contrast sensitivity is already lower for high spatial frequency stimuli.

We tested which of these three mechanisms was underlying the reduction in cortical acuity using extracellular single-unit recordings. Receptive fields were computed by reverse correlation of the response to high contrast sparse checkerboard stimulation. The receptive field sizes were not different between TrkB.T1-EGFP-expressing and wild-type animals, (T1: 21±1 deg, 72 cells; wt: 22±1 deg, 86 cells; p=0.5, t-test, **Supplementary Fig. 5**), excluding the first mechanism.

We next assessed the second mechanism, a reduction in SNR (**Supplementary Fig. 6**). We first considered the spontaneous rate to be related to the noise and the peak response amplitude related to the signal. Peak rates were not significantly different between transgenic and control animals (T1: 13±1 Hz; wt: 14±1 Hz; p=0.5, t-test) and spontaneous rates were even lower in TrkB.T1-EGFP-expressing mice (T1: 4.0±0.6, wt: 6.3±0.8 Hz, p=0.02, t-test). The response index, i.e. (peak rate – spontaneous rate) / peak rate also showed no difference (T1: 0.67±0.04; wt: 0.62±0.03; p=0.3, t-test). A more sophisticated measurement for SNR is the probability that one can correctly determine the onset of a light patch in a neuron's receptive field center based on its response amplitude. We determined this by assessing the area under the receiver operating characteristic (ROC) curve[26] but found no difference between transgenic and control animals (T1: 0.945±0.008; wt: 0.942±0.008; p=0.8, t-test). Also, neither the variation in the response amplitude to drifting gratings (response standard deviation, T1: 2.5±0.5 Hz; wt: 3.3±0.8 Hz; p=0.4, t-test), nor the linear relationship[26] between log response and log response variance (slope, T1: 1.2; wt: 1.3) was different. Therefore, there is no indication for a change in SNR in TrkB.T1-EGFP-expressing mice.

To test whether the third mechanism, a reduction in apparent contrast, was responsible for the lower visual acuity we measured contrast tuning in individual neurons. An example is shown in **Figure 3a**, together with an illustration of the C_{50} point which marks the contrast at which a cell responds at half of its maximal response. The mean C_{50} was markedly higher in TrkB.T1-EGFP animals (T1: 65±4 %, 13 units, 4 animals; wt: 50±4 %, 17 units, 4 animals; p=0.007, t-test, **Fig. 3b**), suggesting reduced apparent contrast in TrkB.T1-EGFP-expressing mice. Normally, latency increases as contrast decreases, often without a proportional loss in response strength[27]. Therefore, we also examined whether the

latency of the peak response to the highest contrast gratings was increased in TrkB.T1-EGFP-expressing mice. This was indeed the case (T1: 0.51±0.06 s; wt: 0.35±0.05 s; p=0.03, one-tailed t-test, **Fig. 3c**). Moreover, the average latency of the peak response to a stimulus in a cell's receptive field center was higher in TrkB.T1-EGFP-expressing animals (T1: 0.164±0.007 s; wt: 0.138±0.004 s; p=0.001, t-test, **Supplementary Fig. 7**). Inspection of the average contrast response curves showed that of *TrkB.T1-EGFP* transgenic animals to be below the wild-type curve (**Fig. 3d**). To confirm that this indicated a reduction in apparent contrast instead of a reduction in response, we fitted the wild-type response curve to the *TrkB.T1-EGFP* mice measurements by scaling its response or contrast (**Fig. 3e**). Reducing contrast by a factor 1.5 provided the best fit (least squared error, contrast scaling: 0.006, response scaling: 0.02). This corroborated the suggestion of a reduced apparent contrast by the increased average C_{50}. Intrinsic signal imaging of the contrast response curve confirmed this. The imaged C_{50} was reduced (T1: 40 ± 3 %; wt: 29 ± 3 %; p = 0.03, t-test, **Supplementary Fig. 8**) and the contrast response curve in *TrkB.T1-EGFP* mice is better fitted by a reduced apparent contrast than by a reduced response (least squared error, contrast scaling: 0.003, response scaling: 0.03, **Fig. 4a**).

We then tested whether the amount of reduction of apparent contrast measured in *TrkB.T1-EGFP* animals is sufficient to explain all the observed loss of acuity and whether a contrast reduction would also preserve responses to low spatial frequency stimuli. We reduced the stimulus contrast by a factor 1.5 (from 90% to 60%), and measured in wild-type animals whether this resulted in a similar reduction in acuity as observed in TrkB.T1-EGFP-expressing mice at 90% contrast. Indeed, acuity at 60% contrast in wild-type animals was reduced to 0.39 cpd versus 0.52 cpd at 90% contrast (p=0.01, paired t-test, **Fig. 4b**). Exactly like in the TrkB.T1-EGFP-expressing animals, there was no significant reduction in the response at 0.1 cpd, while there was in responses to gratings of 0.3 and 0.4 cpd, (p=0.008 and p=0.004, paired t-test, **Fig. 4c-d**). We conclude that the loss of acuity is completely due to a loss of apparent contrast, and no additional cause is needed to explain the phenotype.

Normalization explains interplay of contrast and acuity

While providing a mechanistic explanation for the loss of visual acuity in *TrkB.T1-EGFP* mice, these results did not explain how the reduction of overall synaptic strength in *TrkB.T1-EGFP* mice or the contrast reduction in wild-type mice could leave visual responses to low spatial frequency stimuli unaffected. A possible explanation could lie in contrast normalization occurring in the cortex. For this reason, we employed Heeger's normalization model[28], the standard phenomenological model of V1 responses. It was introduced to describe non-linear response phenomena in V1, such as response suppression by a superimposed additional stimulus and, especially relevant in our context, contrast saturation[29]. We used the model to describe how contrast affects the spatial frequency tuning curve (and vice versa) and

test whether these predictions would explain our experimental data.

In describing the model, we confined ourselves to stimuli that are single sinusoidal gratings of contrast c and spatial frequency f. The unnormalized response A_i of a neuron i is a function that grows linearly with contrast followed by a power law half-rectification, $A_i=max(0, cL_i)^n$, (**Fig. 5a**). The cell's firing rate, R_i, is given by dividing this response A_i by a normalization factor: $R_i=A_i/N$. This normalization factor N reflects the total incoming or local activity and is given by a constant σ^n plus the sum of the unnormalized responses of all local neurons: $N(c, f)=\sigma^n+\Sigma_i A_i$. We assume here that the intrinsic signal response P is proportional to the population firing response $\Sigma_i R_i$, but our conclusions will be valid for any invertible relationship between the two.

At this point, the model already allows a qualitative understanding of why a reduction of contrast or input only reduces high spatial frequency responses. For high contrasts, there is strong local activity at low spatial frequencies and thus strong normalization reducing the responses, while at high spatial frequencies local activity and normalization are weak. At low contrast, the feed-forward drive to the cortex is less at both spatial frequencies, but because the concomitant decrease in normalization is far greater for low spatial frequency responses, these are less reduced than high spatial frequency responses. This concept is illustrated in **Figures 5b-e**, showing the spatial frequency tuning curves of two hypothetical example cells tuned to low and high spatial frequencies at high and intermediate contrasts.

Derivation of model predictions

To test whether the model would also provide an accurate quantitative fit to our intrinsic optical imaging data, we needed to derive an expression for the intrinsic signal response as a function of contrast c and spatial frequency f. To this end, we separated contrast and spatial frequency by defining a function S as the contrast-independent part of the summed unnormalized response by $S(f) = \Sigma_i A_i / c^n = \Sigma_i max(0,c L_i)^n / c^n = \Sigma_i max(0, L_i)^n$. This leads to the normalized population response given by:

$$(*) \qquad P(c, f) = \gamma c^n S(f) / \{ \sigma^n + c^n S(f) \},$$

The constant $\gamma = (\sigma^n/S(f_{low}) + c_{high}^n) / c_{high}^n$, is chosen such that the population response at maximal contrast and lowest spatial frequency is normalized to 1, *i.e.* $P(c_{high}=90\%, f_{low}=0.1 cpd)=1$. For any fixed spatial frequency f, equation (*) reduces to a Naka-Rushton function describing neuronal contrast tuning[29]. The population response $P(c, f)$ obeys the relation $P(c, f)=P(\{S(f)/S(f_{low})\}^{1/n} c, f_{low})$, because the only dependence on f and c in the population response is via the parameter $c^n S(f)$. This means that the population contrast tuning curve at spatial frequency f is identical to the contrast

tuning curve at f_{low} when contrast is rescaled by a factor $\{S(f)/S(f_{low})\}^{1/n}$. An explicit expression of $P(c,f)$ in terms of the experimentally measured parameters σ and n and the acuity at high contrast is given in the **Supplementary Equations**, but is unnecessary for testing the match of model and data.

Normalization model reliably matches experimental data

The model thus predicts that population contrast tuning curves at different spatial frequencies are identical to the contrast tuning curve at 0.05 cpd when the contrast is rescaled appropriately. We confirmed this experimentally (**Fig. 6**). The fit of data and model is clearest in the data of individual mice (**Fig. 6a**). The small variations in shape of the contrast response curves of different mice make the average contrast response curves more linear than the separate curves of individual mice. This effect reduces the difference in scaling fitness of a response and contrast reduction, but the optimal contrast scaling still fit the data much better than an optimal scaling of the response (least squared error $9*10^{-6}$ vs $3*10^{-5}$, 6 mice, **Fig. 6b-d**).

This scaling relationship can be used to construct the spatial frequency tuning curve for any contrast graphically. This is illustrated in **Figures 7a-b**. Through this construction, the model provides a remarkably exact prediction of the spatial frequency tuning curve data obtained in wild-type animals at 60% contrast ($\chi^2(3)=0.42$, p=0.9, χ^2 –test, **Fig. 7c**). Because 60% was also the perceived contrast of the high contrast stimuli in TrkB.T1-EGFP-expressing animals, we could compare the spatial frequency tuning curve measured in these transgenic mice directly to those modeled in control animals. The model also gives an accurate prediction of the *TrkB.T1-EGFP* phenotype at high contrast ($\chi^2(3)=0.42$, p=0.9, χ^2 -test, **Fig. 7d**), showing that it offers a good quantitative understanding of the relationship of contrast and acuity.

DISCUSSION

To study the role of TrkB/BDNF in cortical visual acuity, we investigated synaptic transmission and visual responses in the visual cortex of adult mice with a post-developmental genetic impairment of TrkB signaling restricted to cortical pyramidal cells. TrkB/BDNF-signaling is a well known regulator of synaptic strength in many brain areas[15,18] including V1[30]. We therefore tested whether synaptic strength was reduced in *TrkB.T1-EGFP* transgenic mice using intracellular and local field responses in layer 2/3 to extracellular stimulation in layer 2/3 and layer 4, respectively. Total synaptic strength was indeed reduced for both connection types. In addition to a reduction of the stimulated responses which reflect the balance between excitation and inhibition, we measured an anatomical loss of perisomatic inhibition. The reduction in excitatory transmission was thus larger than the response losses alone suggested. Chronic reduction of

postsynaptic release of BDNF is known to reduce perisomatic inhibition[25]. If this is mediated by a postsynaptic effect on inhibitory synapses, a similar mechanism could be at work in the transgenic mice. Alternatively, the reduction of inhibition could be caused by a homeostatic compensatory mechanism in response to the decreased excitatory transmission.

At first glance, the transgenic animals had a normal visual system despite these synaptic changes. Consistent with previous reports in young mice with deficient TrkB/BDNF signaling[31,32] we found that ocular dominance and its plasticity were unaffected. Responses to low spatial frequency stimuli were unaltered. However, responses to high spatial frequency stimuli were severely reduced or lost. Extracellular recordings showed that this was not explained by changes in signal-to-noise ratios or receptive field sizes. The latter finding is in line with studies in heterozygous BDNF-deficient mice[31] and mice in which TrkB kinase activity was inhibited by a chemical-genetic approach[32]. Single-unit and intrinsic signal measurements, however, revealed that in TrkB.T1-EGFP-expressing animals the average contrast tuning curve could be matched to the wild-type curve by scaling the contrast. Moreover, the selective loss of high spatial frequency responses observed in TrkB.T1-EGFP-transgenic animals could be replicated in wild-type animals when stimuli were presented at a reduced contrast. We conclude that reduced apparent contrast caused this selective deficit. As stimulus contrast correlates with synaptic input amplitude, this provides a logical connection between the effect of reduced TrkB signaling at the cellular level and reduced contrast perception at the systems level. Our results are interesting in the context of previous work showing that forebrain overexpression of BDNF induces an earlier rise of acuity during development[6] which does not require visual experience[13]. Possibly, a BDNF-mediated increase in synaptic strength and contrast gain explains part of this experience-independent increase in acuity in addition to the observed reduction of receptive field sizes in these animals.

Why would reduced apparent contrast selectively affect high spatial frequency responses, leaving those to low spatial frequencies unaffected? Heeger's normalization model describing the effects of gain control in V1[28] such as contrast saturation provides the answer. The model prescribes that responses of individual neurons are normalized by local activity, causing responses to strong stimuli to be diminished more by normalization than those to weak stimuli. When we implemented the natural assumption that the normalization pool displays the same spatial frequency tuning as the general population, the model explained the contrast-induced acuity loss and showed an accurate fit to the phenotype of TrkB.T1-EGFP-expressing animals (**Fig. 7d**) and low contrast measurements in wild-type animals (**Fig. 7c**). A contrast reduction decreases the visual input for high and low spatial frequency stimuli in the same proportion. The reduced feed-forward drive for low spatial frequencies, however, will be masked by a concomitant reduction in the

normalization. At high spatial frequencies, there is little normalization to begin with and a reduction of input hence leads to a drop in response.

Our data thus support an implementation of the normalization model that predicts spatial frequency tuning to be contrast-dependent. How can this be reconciled with previous literature in carnivores and primates implying that spatial frequency tuning in individual neurons is contrast-invariant[29]? The explanation for the discrepancy lies in the fact that the mouse population tuning curve (**Fig. 4c**) already slopes at the lowest spatial frequencies where we measured. The level of normalization thus diminishes at increasing spatial frequencies. In high acuity animals, however, the population tuning at intermediate spatial frequencies is relatively flat compared to that of most individual neurons[33]. This means that neurons tuned to this spatial frequency range will show contrast-invariant spatial frequency tuning. This effect will be augmented by the presence of a cortical spatial frequency map[34]. However, at high spatial frequencies the population tuning curve slopes like the measured mouse curve. For neurons tuned to these high spatial frequencies, the normalization model thus predicts a departure from contrast invariance. This has indeed experimentally been found previously[35,36], but had not been considered as a logical consequence of normalization. The normalization model thus correctly predicts the contrast invariance of intermediate spatial frequency preferring cells of cats and primates and fits the contrast dependence of high spatial frequency preferring cells (**Supplementary Fig. 9 and Supplementary Equations**). We expect that impairment of TrkB/BDNF signaling would also reduce apparent contrast in these animals. Primate and cat contrast sensitivity curves, which give the minimum contrast necessary to detect a specific spatial frequency, are steeper at the high spatial frequency limit compared to the mouse. A similar loss in contrast would thus translate into a milder loss of acuity.

Heeger's model is among the most influential concepts in vision literature. Our data provide further support for its validity, but its biological implementation remains unknown. Response normalization has been hypothesized to be implemented by intracortical GABA-ergic inhibition[37–40], short-term depression in the thalamocortical synapse[41,42], intracortical synaptic depression[43,44] or caused by contrast saturation in LGN responses[45,46]. It is likely that a combination of these mechanisms is responsible for the normalization of cortical responses. Our results show that normalization is not over at the stage of the thalamocortical synapse. Normalization of information arriving in the pyramidal layers certainly occurs, because we found that the specific reduction of synaptic transmission in layer 2/3 in *TrkB.T1-EGFP* transgenic animals was not accompanied by a concomitant reduction in the response to salient stimuli. The normalization mechanism itself, whatever its nature, is unaffected in the *TrkB.T1-EGFP* transgenics as their contrast response curve is fitted with the same saturation level and rectification exponent as used for wild-type mice.

Our findings may have interesting implications for cortical acuity loss in amblyopia or aging. Similar to our observations in *TrkB.T1-EGFP* transgenic mice, acuity loss in aging humans or animals often occurs in the absence of changes in the eye or thalamus and is associated with a specific loss of response amplitude to high spatial frequency stimuli and a rise in VEP latencies[4]. Also the loss of contrast sensitivity in amblyopia[5,47] is reminiscent of our observations in *TrkB.T1-EGFP* transgenic mice. Interestingly, reduction of TrkB/BDNF-signaling[7,8,9] and reduced synaptic strength[48] have also been observed under these conditions and may thus have a causal role. This suggests that the search for therapeutic strategies for these deficiencies should include strategies that increase TrkB/BDNF signaling in the visual cortex. Indeed, antidepressants[12] and environmental enrichment[11,49] both lead to an increase in BDNF signaling in the rodent cortex and positively affect visual acuity. It will be interesting to examine the effects of environmental enrichment or antidepressant treatment on visual acuity in an aged population.

ACKNOWLEDGMENTS

We thank Sacha Nelson for reading the manuscript and, together with Stephen Van Hooser, for visual stimulation software, Arianna Maffei and Chris de Zeeuw for discussions, Robin Hartman for assistance with monocular deprivation, Svetlana Škulj-Živkovic, Sitha Scheltinga and Sarra Riahi for genotyping, and Chris Pool and Joop van Heerikhuize for puncta analysis macros. CL, JAH and JMH were supported by SenterNovem BSIK-grant 03053. SC was supported by Rotterdamse Vereniging Blindenbelangen, ANVVB, and Stichting Blindenhulp. CL and MHS were supported by a ZonMW VIDI-grant.

AUTHOR CONTRIBUTIONS

CNL made the *TrkB.T1-EGFP* mice. JAH and CNL devised the experiments, developed wrote the manuscript. JAH performed the in vivo experiments and implemented the normalization model. MHS carried out the slice experiments. SC analyzed PV-puncta. JMH assisted with imaging.

Figure legends

Figure 1. Expression of TrkB.T1-EGFP in pyramidal neurons of the adult visual cortex causes reduced synaptic strength. **(a)** Sagittal slice showing expression at postnatal day 68 in cortex and hippocampus. Fluorescence in the thalamus is limited to axons coming from the cortex and hippocampus. **(b)** Coronal cross-section of occipital cortex shows expression of TrkB.T1-EGFP mainly in extragranular layers. **(c)** Experimental setup for **d-e**. Whole-cell patch clamp

recording in layer 2/3 coupled to electrical stimulation displaced 200 µm in layer 2/3 **(d)** Example average response to 50 µA electrical stimulation. **(e)** Average layer 2/3 to 2/3 input-output (IO) curves show a reduced response in *TrkB.T1-EGFP* mice. **(f)** Experimental setup for **g-h**. LFP recording electrode in layer 2/3 of visual cortical slice coupled to electrical stimulation in layer 4. **(g)** Example average response to 180 µA stimulation in a wild-type and a *TrkB.T1-EGFP* mouse. **(h)** Average layer 4 to 2/3 input-output curves show a reduced response in TrkB.T1-EGFP mice. (error bars denote SEMS and *: $p<0.05$; **: $p<0.01$, t-test)

Figure 2. Acuity is reduced in V1 of TrkB.T1-EGFP-expressing mice. **(a,b)** Example intrinsic signal responses to a range of spatial frequencies in the visual cortex of a wild-type mouse. Scale bar is 1mm. **(c)** Average high spatial frequency cut-offs are reduced in TrkB.T1-EGFP-expressing mice compared to controls. **(d)** Average intrinsic signal responses for wild-type and *TrkB.T1-EGFP* transgenic animals. Response to the lowest spatial frequency is not significantly reduced. (error bars denote SEMS and *: $p<0.05$; **: $p<0.01$, t-test).

Figure 3. Apparent contrast is reduced in *TrkB.T1-EGFP* mice. **(a)** Example single-unit contrast response curve. C_{50} is interpolated from a Naka-Rushton fit. **(b)** C_{50} is higher in *TrkB.T1-EGFP* mice. **(c)** Peak latency to the high contrast gratings is longer in *TrkB.T1-EGFP* mice. **(d)** Average population response curves from single-unit recordings, normalized to wild-type response and fitted with Naka-Rushton curves. **(e)** Best fit to *TrkB.T1-EGFP* data with the wild-type curve (solid line) is achieved by reducing contrast (dashed line), rather than by reducing response strength (dotted line). (error bars denote SEMS and *: $p<0.05$; **: $p<0.01$, t-test)

Figure 4. Apparent contrast reduction in *TrkB.T1-EGFP* mice explains acuity loss. **(a)** Intrinsic signal recordings confirm reduction of contrast in *TrkB.T1-EGFP* mice. Contrast tuning curve of *TrkB.T1-EGFP* is best fitted by scaling the contrast of the wild-type tuning curve rather than the response (least squared error, contrast scaling: 0.003, response scaling: 0.033). **(b-d)** Contrast reduction decreases acuity and mimics *TrkB.T1-EGFP* phenotype. **(b)** Intrinsic signal measurements in wild-type animals show cortical acuity is lower at 60% compared to 90% contrast. **(c-d)** The loss of response to high spatial frequency stimuli and the absence of a response reduction at low spatial frequency induced by contrast reduction from 90% to 60% matches the *TrkB.T1-EGFP* acuity phenotype. Lines are linear-threshold fits to wild-type data (error bars denote SEMS and *: $p<0.05$; **: $p<0.01$, t-test).

Figure 5. Normalization model explains the differential effect of reduced contrast on responses to high and low spatial frequency stimuli. **(a)** V1 Normalization model. Neuron *i* performs an operation on the stimulus that is linear in contrast. This operation is followed by a power law half-rectification. This unnormalized response A_i is normalized by division with an activity pool N, which only depends on stimulus contrast and spatial frequency, to give the cell's firing rate R_i. Firing rates of all cells together determine the population response P. **(b)** Hypothetical examples of unnormalized responses of

a cell preferring low spatial frequencies (top) and one preferring high spatial frequencies (bottom). A reduction in contrast strongly reduces the responses, without altering the tuning preferences or their relative response strengths. **(c)** High contrast, low spatial frequency stimuli evoke large population response and thus large normalization. **(d,e)** Firing rates of hypothetical cells of **b** after normalization by **c** and population response show that the responses at high spatial frequencies are much more dependent on contrast.

Figure 6. Imaging confirms the model's prediction that population contrast tuning curves at different spatial frequencies are identical when contrast is rescaled. **(a)** Contrast responses at 0.1, 0.2 and 0.4 cpd in a single mouse are well fitted by scaling the contrast of the 0.05 cpd contrast tuning curve. **(b-d)** Contrast scaling of average 0.05 cpd contrast tuning curve fits contrast response curves at 0.1, 0.2 and 0.4 cpd better than scaling the response. **(c)** Optimally scaled contrast for spatial frequency of **b** to match the 0.05 cpd response curve. **(d)** Optimally scaled response for each spatial frequency of **b** to match the 0.05 cpd response curve. (error bars denote SEMS).

Figure 7. Model predicts population spatial frequency and contrast relationships in wild-type and TrkB.T1-EGFP mice. **(a,b)** From measurements of the contrast tuning at 0.1 cpd **(a)** and the spatial frequency tuning at 90% contrast **(b)**, the model predicts the response at any combination of contrast and spatial frequency, by scaling the contrast of the measured contrast tuning curve in **a** to match the 90% contrast response of the requested spatial frequency in **b**. Horizontal lines show a construction of the predicted response to a 60% contrast grating of 0.2 cpd: the contrast of the contrast tuning curve of 0.1 cpd is scaled such that at 90% the response is identical to the response measured for the high contrast spatial frequency curve in **b**. After scaling, the contrast tuning curve response at 60% gives the desired value. **(c,d)** The model's predicted spatial frequency tuning curve at 60% contrast closely matches the 60% contrast measurements in wild-type animal and the 90% contrast measurements in *TrkB.T1-EGFP* animals. (error bars denote SEMS)

METHODS

Production of transgenic mice. Mice with a Cre-dependent *TrkB.T1-EGFP* transgene (TLT-817) were described previously[16]. *TrkB.T1-EGFP* transgenic animals were crossed to animals from the *G35-3-Cre* line[20]. All lines had been kept on a C57BL/6 background for at least 6 generations. Cre-negative and/or *loxP*-Stop-*loxP*-negative littermates were used as controls. Genotyping was done by PCR using primers for Cre-recombinase, and the *loxP*-Stop-*loxP* cassette. Most experimental animals were perfused with 4% PFA (www.sigmaaldrich.com) in PBS to confirm the genotype after recording.

All experiments were approved by the institutional animal care and use committee of the Royal Netherlands Academy of Arts and Sciences.

Histology and immunohistochemistry. Mature animals were perfused and brains dissected and sliced in 50 μm coronal sections using a Leica VT1000S vibratome (www.leica.com). We double-stained free-floating sections using mouse anti-NeuN antibodies (1:500, Chemicon, www.millipore.com) and rabbit anti-parvalbumin (1:1000, www.swant.com) followed by Alexa 488 conjugated goat anti-mouse antibodies (1:500, Molecular Probes, www.invitrogen.com) and Alexa 568 conjugated goat anti-rabbit antibodies (1:500, Molecular Probes). We imaged these sections with HeNe (543 nm) and Argon (488 nm) lasers. Images were acquired as non-overlapping single planes with 63x oil immersion objective at a scaling of 70 nm and a pinhole of 80 μm on a CLSM 510 Meta confocal microscope (www.zeiss.com). Parvalbumin puncta lying within 2 μm of the border around NeuN-positive nuclei of layer 2/3 cells in V1 were counted using a custom-made macro in ImagePro (www.mediacy.com). Analysis was carried out blind to genotype. We sliced the brains of a few animals sagitally to determine the spatial and temporal expression pattern of the transgene. Images of these slices were acquired with a 10x objective on an Axioplan 2 microscope (www.zeiss.com). Contrast range was stretched linearly for the entire images by Gimp (www.gimp.org).

Optical imaging of intrinsic signal. Mice between two months and one year old were imaged as described previously[10]. Mice were anesthetized by an intraperitoneal injection of urethane (www.sigmaaldrich.com; 200 mg/ml saline, 2 g/kg). Atropine sulphate (0.05 mg/ml in saline, 0.1 mg/kg) was injected subcutaneously to reduce mucous excretions. We resected the scalp, illuminated the skull with 700 nm light, and acquired images using an Optical Imager 3001 system (www.opt-imaging.com). A gamma-corrected CRT monitor was placed 16 cm from the mouse covering the mouse' visual field from −15 to 75 deg horizontally and from −44 to 44 deg vertically. Background luminance was 5 cd/m^2. Spatial frequency and contrast tuning measurements were made using 3 s long presentations of sinusoidal

gratings contrast-reversing at 2 Hz, changing direction every 0.75 s, presented on a gray background. The stimuli covered only the superior nasal quarter of the monitor and were presented to the contralateral (right) eye exclusively. Forty or more presentations of each stimulus were averaged. After each stimulus the screen was gray for 2 s followed by a 1 s presentation of the same stimulus in the inferior nasal monitor quadrant. This was a 'reset' signal for the intrinsic signal in the previously activated part of the cortex, and was followed by a gray screen for at least 15 s. Spatial frequency measurements for **Figure 2** were made with 90% contrast gratings of randomly alternating between 0.1, 0.2, 0.3, 0.4, 0.5 and 0.7 cpd. Spatial frequency measurements for **Figure 4** were made using the same spatial frequencies randomly presented at 60% and 90% contrasts. Cortical acuity was determined by the zero-crossing of a least squares fit with a threshold-linear function. Contrast measurements of **Figure 4a** were made with randomly interleaved gratings of 0.1 or 0.4 cpd at 20, 40, 60, 75 and 90% contrast. **Figure 6** contains the responses to randomly interleaved gratings of 0.05, 0.1, 0.2 and 0.4 cpd at 20, 40, 60 and 90% contrast. Each of the stimuli for **Figure 6** was followed after 3 s by a short 1 s presentation of a 0.1 cpd, 90% contrast grating shown at the same location to avoid adaptation effects.

Ocular dominance plasticity. Ocular dominance was measured by intrinsic signal imaging of the response to alternating visual stimulation of the left and right eye by computer-controlled shutters. Every 17 s one of the shutters opened and a visual stimulus was presented for 3 s in the upper nasal quadrant of the screen. The stimulus was a 90% contrast square-wave grating of 0.05 cpd drifting at 2Hz and changing direction every 0.6s. The shutter would stay open for the entire 6-s period of acquisition. Trials during which both shutters remained closed were interleaved to verify that the shutters completely blocked vision in both eyes. Forty responses to stimuli to each eye were recorded and averaged. The imaged Ocular Dominance Index was defined as the iODI = (contra response – ipsi response) / (contra response + ipsi response). In a subset of the animals, right eyelids were sutured closed under isoflurane anesthesia seven days before imaging, as previously described[10]. The sutured eyelid was reopened at the start of the imaging session.

In vivo electrophysiology. We used mice between six months and one year old for acute extracellular recording experiments. Mice were anesthetized by an intraperitoneal injection of urethane (200 mg/ml saline, 1.2 g/kg) supplemented by a subcutaneous injection of chlorprothixene (www.sigmaaldrich.com; 4 mg/ml distilled water, 8 mg/kg). We injected atropine sulphate (0.05 mg/ml, 0.1mg/kg) and dexamethasone (5 mg/ml, 4 mg/kg) subcutaneously to reduce mucous excretions and to prevent cortical edema, respectively. With a conical dental drill one or more small holes were made in the skull above V1, 2.9 mm lateral and 0.5 anterior to cranial landmark lambda. Most single-unit recordings of the response to a sparse checkerboard were made using 10 MOhm tungsten micro-electrodes (FHC, www.fh-co.com). Contrast tuning curves and some receptive field size were measured with glass-coated tungsten 1

MOhm micro-electrodes (Nano Bio Sensors, www.nano-biosensors.com). Stimuli were projected by a gamma-corrected PLUS U2-X1130 DLP beamer (www.plus-america.com) in a 70x50 cm area on a large backprojection screen (www.macada-innovision.com), positioned 50 cm away from the mouse. The reverse correlation stimulus was a 5 minute-long presentation of a 7x5 grid of square black and white patches in a 34:1 ratio, changing at 5 frames per second. Average patch extent was 8x8 degrees of visual angle. The receptive field size was taken as the approximate extend of all patches which were more than 3 standard deviations away from the mean intensity in the spike-triggered average. We determined contrast tuning with five times repeated 2 second-long presentations of full screen square wave gratings of 0.05 cpd, drifting at 1 Hz in one of the four cardinal directions, shown at 30, 50, 70, 90 and 95% contrast. Background luminance was 0.2 kcd/m^2. Recordings and analysis were done blind to genotype. Visual stimulation and analysis software for imaging and electrophysiology was written in Matlab (www.mathworks.com) and used the Psychophysics Toolbox (www.psychtoolbox.org).

Slice electrophysiology

Mice (4−6 month old) were anesthetized by isoflurane and decapitated. Subsequently, brains were chilled in ice-cold carbogenated (95% O_2/5% CO_2) sucrose-based artificial cerebrospinal fluid (ACSF), containing 3.5 mM KCl, 2.4 mM $CaCl_2$, 1.3 mM $MgSO_4$, 1.2 mM KH_2PO_4, 10 mM glucose, 26 mM $NaHCO_3$, and 212.5 mM sucrose. 300 μm coronal slices of V1 were prepared using a vibrating microtome (www.microm-online.com). Slices were stored in submerged chambers containing carbogenated normal ACSF comprising 125 mM NaCl, 3 mM KCl, 2 mM $MgSO_4$, 2 mM $CaCl_2$, 10 mM glucose, 1.20 mM NaH_2PO_4 and 26 mM $NaHCO_3$ (305 mOsm and pH 7.3), and recorded at 32 ± 0.5 °C under an Axioskop FS upright microscope equipped with infrared Hoffman Modulation Contrast optics (www.zeiss.com) and VX 45 IR-Camera (www.optronis.com).

Layer 2/3 to 2/3 synaptic strength. We patched cells by borosilicate glass patch-pipettes (4−5 MΩ) filled with K-gluconate internal solution containing 154 mM K-gluconate, 1 mM KCl, 0.5 mM EGTA, 10 mM Hepes, 4 mM Mg-ATP, 4 mM phosphocreatine, 0.4 mM GTP (0.290 mOsm and pH 7.3). Cell type was confirmed by the firing pattern in response to depolarizing current steps. In whole-cell configuration, we recorded evoked responses using a patch-clamp amplifier (MultiClamp 700A, Axon Instruments, www.moleculardevices.com) while holding the membrane potential at –70 mV. We took care that series resistance remained <15 MΩ. Recordings with more than 30% change in input resistance were excluded. A glass microelectrode filled with ACSF was placed around 200 μm lateral to the recording site under the following criteria: with 20 μA of stimulation a detectable response was recorded; the response was graded and time to peak response was ≤5 ms; no inhibitory component (upward response) was recorded either in the beginning

or at the end of the trace; the inward current was clearly separated from the stimulation artifact (no direct leakage of current into the dendrite). Electrical stimulation was given at a frequency of 0.1 Hz (6 traces for each stimulation) with a duration of 200 μs. For paired pulse ratio measurements, two pulses, spaced 25 ms apart, were given at an intensity which produced a response of approximately 150 pA. Signals were low-pass filtered at 3.0 KHz, digitized at 10 KHz with a Digidata 1200, and recorded by Clampex 8 software (Axon Instruments). Clampfit 9 (Axon Instruments) was used for analyzing evoked responses. The average of 6 evoked responses was used for comparisons.

Layer 4 to 2/3 synaptic strength. We filled glass microelectrodes with the extracellular solution and placed them in the middle of layer 2/3. A bipolar stimulating electrode (25 μm platinum/iridium CE2C55 FHC, www.fh-co.com) was positioned in layer 4, such that with 15 μA of stimulation a detectable response was recorded. For paired pulse ratio recordings, we used a stimulus intensity which caused half the maximum response obtained in the response curve measurement. Electrical stimulation and analysis were otherwise identical to the protocol used to assess layer 2/3 to 2/3 connectivity.

Statistical analysis and contrast tuning curve fitting. Two-tailed unpaired Student's t-tests were used for all comparisons unless otherwise stated. Contrast tuning curves were fit with a Naka-Rushton curve by minimizing the least squared error using a Nelder-Mead procedure in Matlab. A null-response point at 1% contrast was added to constrain the fit. Minimization was initiated with semisaturation constant $\sigma = 0.4$ and exponent $n = 2$. C_{50}, the contrast where the response is half its maximum, was determined from the fit.

1. Ress, D. & Heeger, D.J. Neuronal correlates of perception in early visual cortex. *Nat. Neurosci.* **6**, 414-420 (2003).

2. Gianfranceschi, L., Fiorentini, A. & Maffei, L. Behavioural visual acuity of wild-type and bcl2 transgenic mouse. *Vision Res.* **39**, 569-574 (1999).

3. Spekreijse, H. Comparison of acuity tests and pattern evoked potential criteria: two mechanisms underly acuity maturation in man. *Behav. Brain Res.* **10**, 107-117 (1983).

4. Spear, P.D. Neural bases of visual deficits during aging. *Vision Res.* **33**, 2589-2609 (1993).

5. Barrett, B.T., Bradley, A. & McGraw, P.V. *Neuroscientist* **10**, 106-117 (2004).

6. Huang, Z.J. et al. BDNF regulates the maturation of inhibition and the critical period of plasticity in mouse visual cortex. *Cell* **98**, 739-755 (1999).

7. Katoh-Semba, R., Semba, R., Takeuchi, I.K. & Kato, K. Age-related changes in levels of brain-derived neurotrophic factor in selected brain regions of rats, normal mice and senescence-accelerated mice: a comparison to those of nerve growth factor and neurotrophin-3. *Neurosci. Res.* **31**, 227-234 (1998).

8. Bozzi, Y. et al. Monocular deprivation decreases the expression of messenger RNA for brain-derived neurotrophic factor in the rat visual cortex. *Neuroscience* **69**, 1133-1144 (1995).

9. Rossi, F.M., Bozzi, Y., Pizzorusso, T., Maffei, L. Monocular deprivation decreases brain-derived neurotrophic factor immunoreactivity in the rat visual cortex. *Neuroscience*. **90**, 363-368 (1999).

10. Heimel, J.A., Hartman, R.J., Hermans, J.M. & Levelt, C.N. Screening mouse vision with intrinsic signal optical imaging. *Eur. J. Neurosci.* **25**, 795-804 (2007).

11. Sale, A. et al. Environmental enrichment in adulthood promotes amblyopia recovery through a reduction of intracortical inhibition. *Nat. Neurosci.* **10**, 679-681 (2007).

12. Maya Vetencourt, J.F. et al. The antidepressant fluoxetine restores plasticity in the adult visual cortex. *Science* **320**, 385-388 (2008).

13. Gianfranceschi, L. et al. Visual cortex is rescued from the effects of dark rearing by overexpression of BDNF. *Proc. Natl. Acad. Sci. USA.* **100**, 12486-12491 (2003).

14. Huang, E.J. & Reichardt, L.F. Neurotrophins: roles in neuronal development and function. *Annu. Rev. Neurosci.* **24**, 677-736 (2001).

15. Lu, B. Acute and long-term synaptic modulation by neurotrophins. *Prog. Brain Res.* ***146***, 137-150 (2004).

16. Chakravarthy, S. et al. Postsynaptic TrkB signaling has distinct roles in spine maintenance in adult visual cortex and hippocampus. *Proc. Natl. Acad. Sci. USA.* **103**, 1071-1076 (2006).

17. McAllister, A.K., Katz, L.C. & Lo, D.C. Neurotrophins and synaptic plasticity. *Annu. Rev. Neurosci.* **22**, 295–318 (1999).

18. Poo, M.M. Neurotrophins as synaptic modulators. *Nat. Rev. Neurosci.* **2**, 24–32 (2001).

19. Eide, F.F. et al. Naturally occurring truncated trkB receptors have dominant inhibitory effects on brain-derived neurotrophic factor signaling. *J. Neurosci.* **16**, 3123-3129 (1996).

20. Sawtell, N.B. et al. NMDA receptor-dependent ocular dominance plasticity in adult visual cortex. *Neuron* **38**, 977-985 (2003).

21. Dahlhaus, M.et al. Notch1 Signaling in Pyramidal Neurons Regulates Synaptic Connectivity and Experience-Dependent Modifications of Acuity in the Visual Cortex, *J. Neurosci*. **28**, 10794-10802 (2008).

22. Gordon, J.A. & Stryker, M.P. Experience-dependent plasticity of binocular responses in the primary visual cortex of the mouse. *J. Neurosci.* **16**, 3274-3286 (1996).

23. Li, Y.X., Xu, Y., Ju, D., Lester, H.A., Davidson, N. & Schuman, E.M. Expression of a dominant negative TrkB receptor, T1, reveals a requirement for presynaptic signaling in BDNF-induced synaptic potentiation in cultured hippocampal neurons. *Proc. Natl. Acad. Sci. USA.* **95**, 10884-10889 (1998).

24. Binzegger, T., Douglas, R.J. & Martin, K.A. A quantitative map of the circuit of cat primary visual cortex. *J Neurosci*. **24**, 8441-53 (2004).

25. Kohara, K., Yasuda, H., Huang, Y., Adachi, N., Sohya, K. & Tsumoto, T. A local reduction in cortical GABAergic synapses after a loss of endogenous brain-derived neurotrophic factor, as revealed by single-cell gene knock-out method. *J Neurosci.* **27**, 7234-44 (2007).

26. Bradley, A., Skottun, B.C., Ohzawa, I., Sclar, G. & Freeman, R.D. Visual orientation and spatial frequency discrimination: a comparison of single neurons and behavior. *J. Neurophysiol.* **57**, 755-772 (1987).

27. Albrecht, D.G., Geisler, W.S., Frazor, R.A. & Crane, A.M. Visual cortex neurons of monkeys and cats: temporal dynamics of the contrast response function. *J. Neurophysiol.* **88**, 888-913 (2002).

28. Heeger, D.J. Normalization of cell responses in cat striate cortex. *Vis. Neurosci.* **9,** 181-197 (1992).

29. Albrecht, D.G. & Hamilton, D.B. Striate cortex of monkey and cat: contrast response function. *J. Neurophysiol.* **48**, 217-237 (1982).

30. Bartoletti, A. et al. Heterozygous knock-out mice for brain-derived neurotrophic factor show a pathway-specific impairment of long-term potentiation but normal critical period for monocular deprivation. *J Neurosci.* **22**, 10072-10077 (2002).

31. Kaneko, M., Hanover, J.L., England, P.M. & Stryker, M.P. TrkB kinase is required for recovery, but not loss, of cortical responses following monocular deprivation. *Nat. Neurosci.* **11**, 497-504 (2008).

32. Carmignoto, G., Pizzorusso, T., Tia, S. & Vicini, S. Brain-derived neurotrophic factor and nerve growth factor potentiate excitatory synaptic transmission in the rat visual cortex. *J. Physiol.* **498**, 153-164 (1997).

33. Heimel, J.A., Van Hooser, S.D. & Nelson, S.B. Laminar organization of response properties in primary visual cortex of the gray squirrel (Sciurus carolinensis). *J Neurophysiol.* 94, 3538-3554 (2005).

34. Issa, N.P., Trepel, C. & Stryker, M.P. Spatial frequency maps in cat visual cortex. *J. Neurosci.* **20**, 8504-8514 (2000).

35. Skottun, B.C., Bradley, A. & Ramoa, A.S. Effect of contrast on spatial frequency tuning of neurones in area 17 of cat's visual cortex. *Exp. Brain Res.* **63**, 431-435 (1986).

36. Sceniak, M.P., Hawken, M.J. & Shapley, R. Contrast-dependent changes in spatial frequency tuning of macaque V1 neurons: effects of a changing receptive field size. *J. Neurophysiol.* **88**, 1363-1373 (2002).

37. Morrone, M.C., Burr, D.C. & Speed, H.D. Cross-orientation inhibition in cat is GABA mediated. *Exp. Brain Res.* **67**, 635-644 (1987).

38. Carandini, M. & Heeger, D.J. Summation and division by neurons in primate visual cortex. *Science* **264**, 1333-1336 (1994).

39. Carandini, M., Heeger, D.J. & Movshon, J.A. Linearity and normalization in simple cells of the macaque primary visual cortex. J. Neurosci. 17, 8621-44 (1997).

40. Sengpiel, F. & Vorobyov, V. Intracortical origins of interocular suppression in the visual cortex. *J. Neurosci.* **25**, 6394-6400 (2005).

41. Kayser, A, Priebe, N.J. & Miller, K.D. Contrast-dependent nonlinearities arise locally in a model of contrast-invariant orientation tuning. *J. Neurophysiol.* **85**, 2130-2149 (2001).

42. Carandini, M., Heeger, D.J. & Senn, W. A synaptic explanation of suppression in visual cortex. *J Neurosci.* **22**, 10053-10065 (2002).

43. Chance, F.S., Nelson, S.B. & Abbott, L.F. Synaptic depression and the temporal response characteristics of V1 cells. *J. Neurosci.* **18**, 4785-4799 (1998).

44. van Rossum, M.C., van der Meer, M.A., Xiao, D. & Oram, M.W. Adaptive integration in the visual cortex by depressing recurrent cortical circuits. *Neural Comput.* **20**, 1847-1872 (2008).

45. Priebe, N.J. & Ferster, D. Mechanisms underlying cross-orientation suppression in cat visual cortex. *Nat. Neurosci.* **9,** 552-561 (2006).

46. Li, B., Thompson, J.K., Duong, T., Peterson, M.R. & Freeman, R.D. Origins of cross-orientation suppression in the visual cortex. *J. Neurophysiol.* **96**, 1755-1764 (2006).

47. Bradley, A. & Freeman, R.D. Contrast sensitivity in anisometropic amblyopia. *Invest. Ophthalmol. Vis. Sci.* **21**, 467-476 (1981).

48. Heynen, A.J., Yoon, B.J., Liu, C.H., Chung, H.J., Huganir, R.L. & Bear, M.F. Molecular mechanism for loss of visual cortical responsiveness following brief monocular deprivation. *Nat. Neurosci.* **6,** 854-862 (2003)**.**

49. Bartoletti, A., Medini, P., Berardi, N. & Maffei, L. Environmental enrichment prevents effects of dark-rearing in the rat visual cortex. *Nat. Neurosci.* **7**, 215-216 (2004).

Supplementary Information Titles

Journal: Nature Neuroscience

Article Title: Contrast gain control and cortical TrkB signaling shape visual acuity

Corresponding author: J. Alexander Heimel

Supplementary Figure 1 Construction of mice expressing TrkB.T1-EGFP in pyramidal neurons of the adult visual cortex.

Supplementary Figure 2 Reduced perisomatic inhibitory input to pyramidal neurons in TrkB.T1-EGFP expressing mice.

Supplementary Figure 3 Adult ocular dominance plasticity is unchanged in *TrkB.T1-EGFP* mice.

Supplementary Figure 4 Possible mechanisms underlying a loss of acuity.

Supplementary Figure 5 No changes in receptive field size in *TrkB.T1-EGFP* mice.

Supplementary Figure 6 No changes in signal-to-noise ratio in *TrkB.T1-EGFP* mice.

Supplementary Figure 7 Peak response latency is longer in *TrkB.T1-EGFP* mice.

Supplementary Figure 8 Imaged C_{50} values are increased in *TrkB.T1-EGFP* mice.

Supplementary Figure 9 Loss of high spatial frequency responses with a reduction of contrast is also apparent in cat and macaque literature.

Supplementary Equations

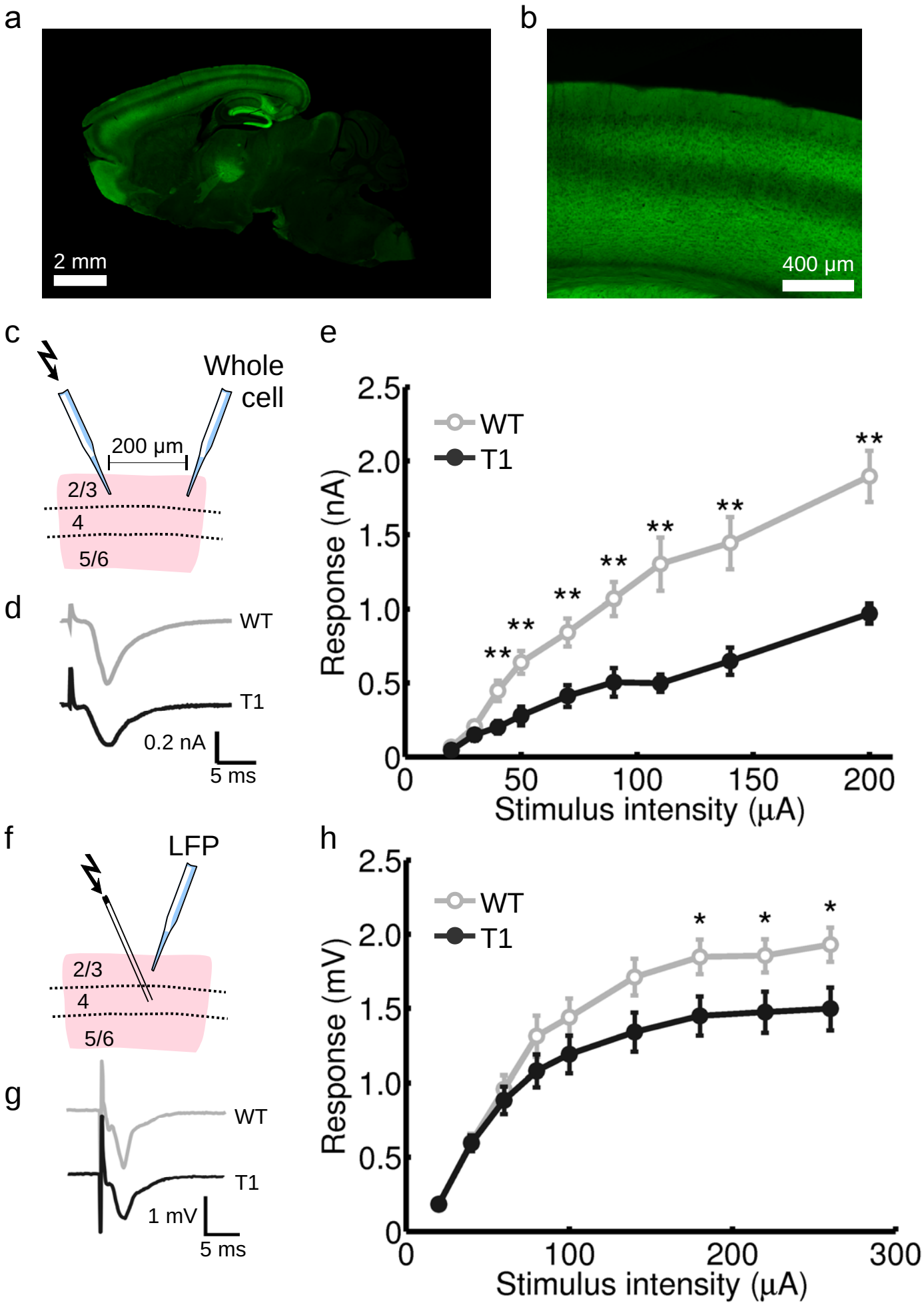
a
2 mm
b
400 μm
c
Whole cell
200 μm
2/3
4
5/6
d
WT
T1
0.2 nA
5 ms
e
Response (nA)
WT
T1
Stimulus intensity (μA)
f
LFP
2/3
4
5/6
g
WT
T1
1 mV
5 ms
h
Response (mV)
WT
T1
Stimulus intensity (μA)

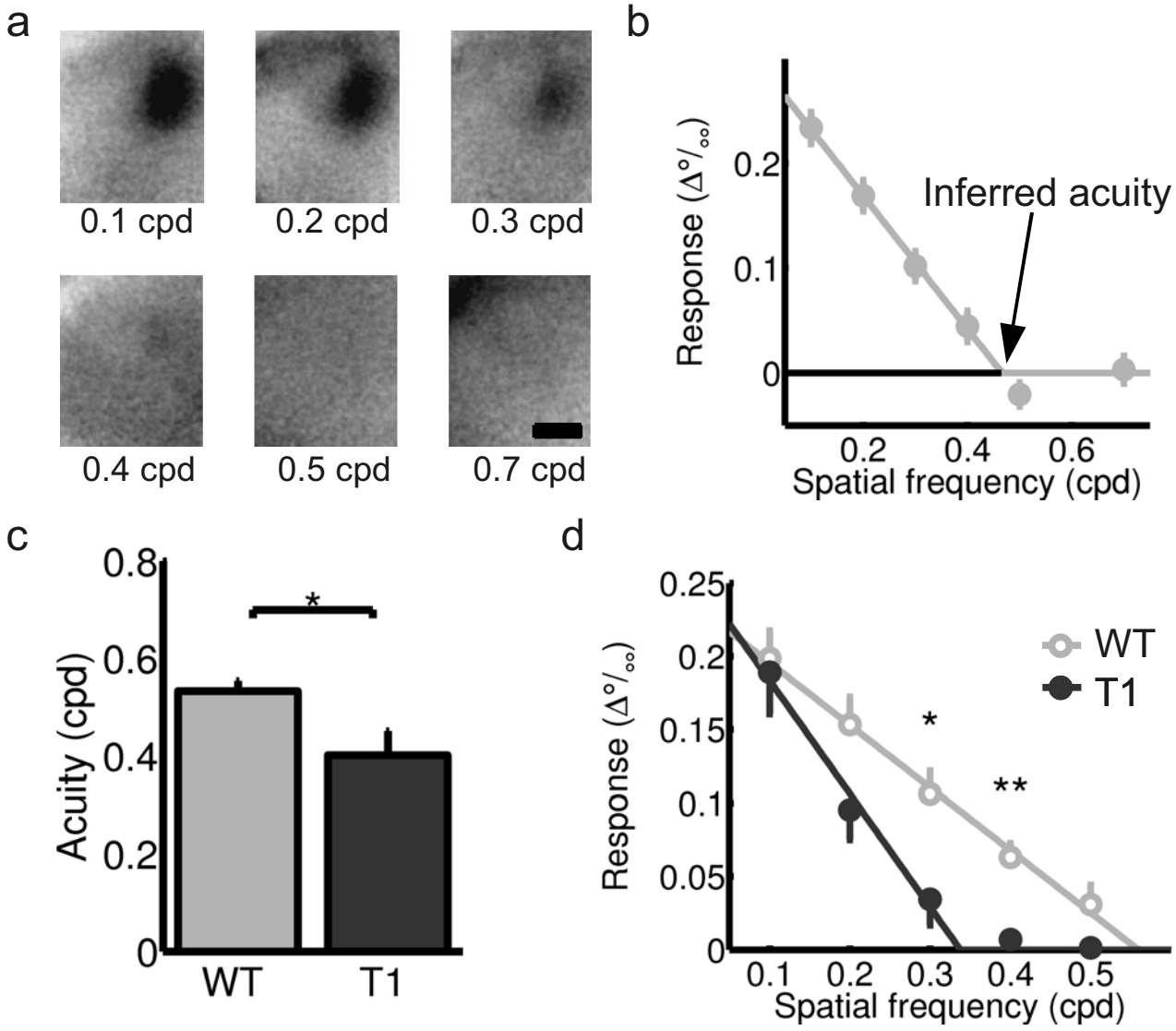
a
0.1 cpd
0.2 cpd
0.3 cpd
0.4 cpd
0.5 cpd
0.7 cpd
b
Response (Δ°/₀₀)
0.2
0.1
0
Inferred acuity
0.2
0.4
0.6
Spatial frequency (cpd)
c
Acuity (cpd)
0.8
0.6
0.4
0.2
0
*
WT
T1
d
Response (Δ°/₀₀)
0.25
0.2
0.15
0.1
0.05
0
WT
T1
*
**
0.1
0.2
0.3
0.4
0.5
Spatial frequency (cpd)

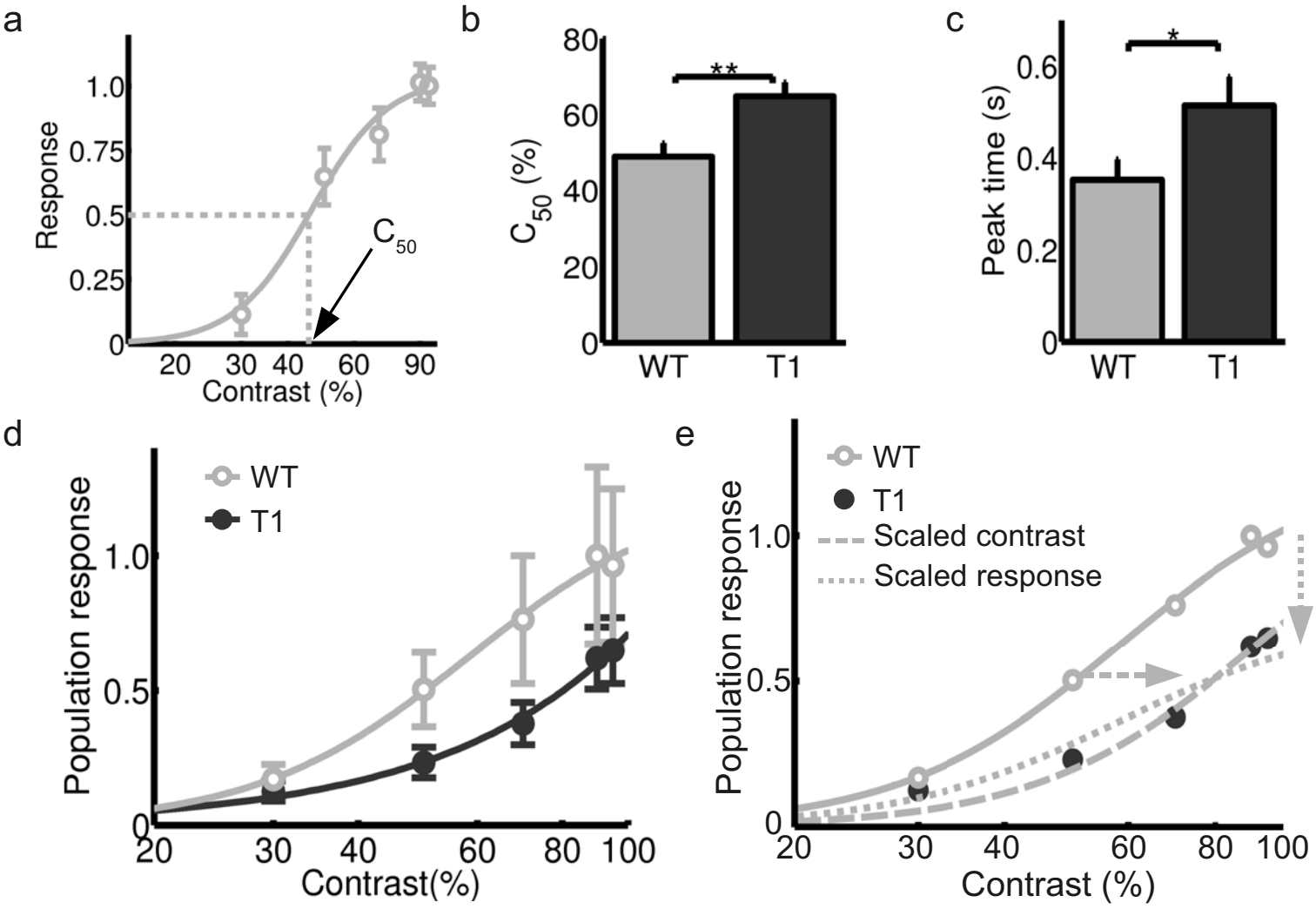
a
Response
1.0
0.75
0.5
0.25
0
C50
20
30
40
60
90
Contrast (%)
b
C50 (%)
80
60
40
20
0
**
WT
T1
c
Peak time (s)
0.6
0.4
0.2
0
*
WT
T1
d
Population response
WT
T1
1.0
0.5
0
20
30
40
60
80
100
Contrast(%)
e
Population response
WT
T1
Scaled contrast
Scaled response
1.0
0.5
0
20
30
40
60
80
100
Contrast (%)

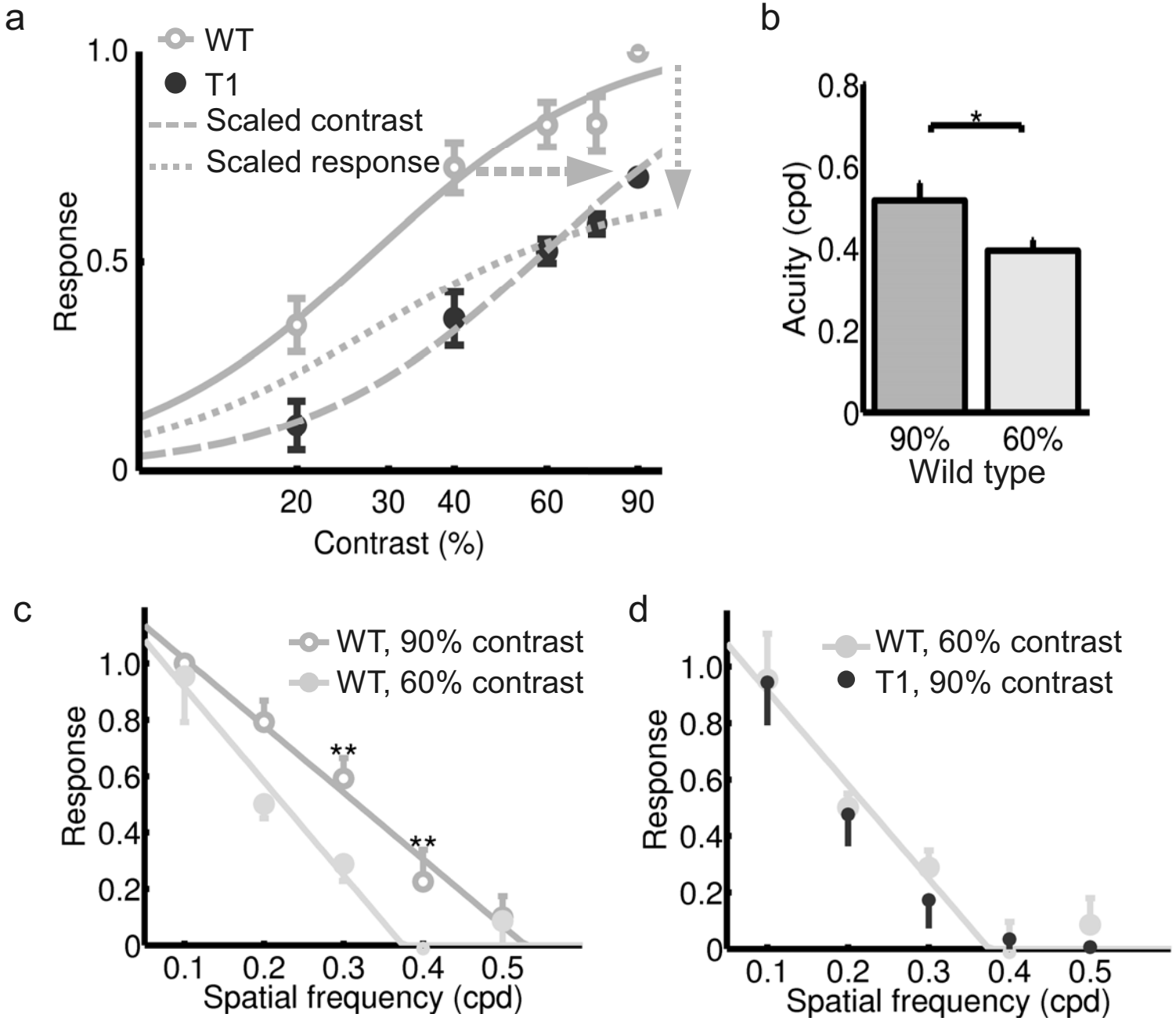
a
WT
T1
Scaled contrast
Scaled response
Response
1.0
0.5
0
20
30
40
60
90
Contrast (%)
b
Acuity (cpd)
0.8
0.6
0.4
0.2
0
*
90%
60%
Wild type
c
WT, 90% contrast
WT, 60% contrast
Response
1.0
0.8
0.6
0.4
0.2
0
**
**
0.1
0.2
0.3
0.4
0.5
Spatial frequency (cpd)
d
WT, 60% contrast
T1, 90% contrast
Response
1.0
0.8
0.6
0.4
0.2
0
0.1
0.2
0.3
0.4
0.5
Spatial frequency (cpd)

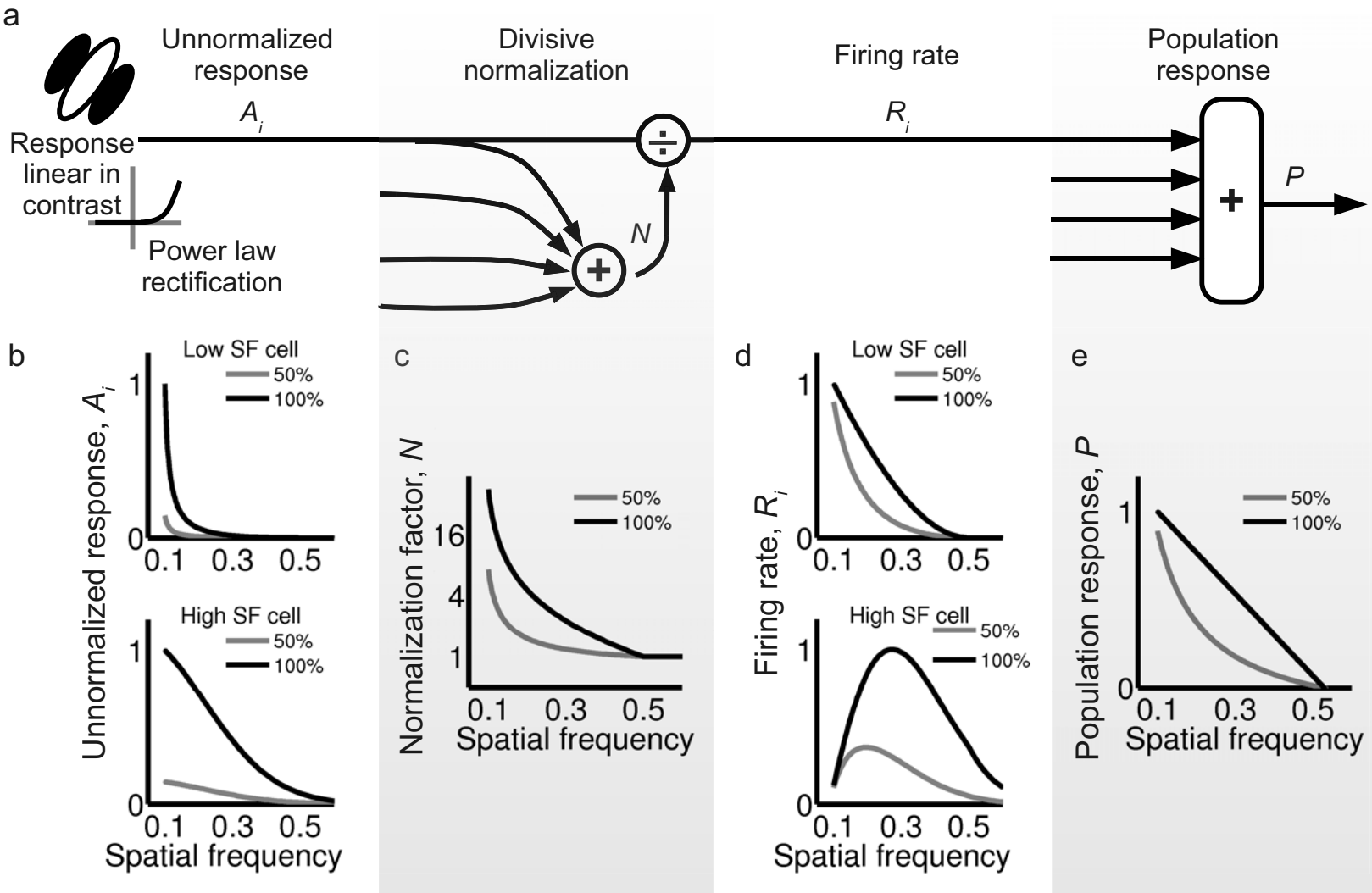
a
Unnormalized response
A_i
Divisive normalization
Firing rate
R_i
Population response
Response linear in contrast
Power law rectification
N
P
b
Low SF cell
50%
100%
Unnormalized response, A_i
High SF cell
Spatial frequency
c
Normalization factor, N
d
Firing rate, R_i
e
Population response, P

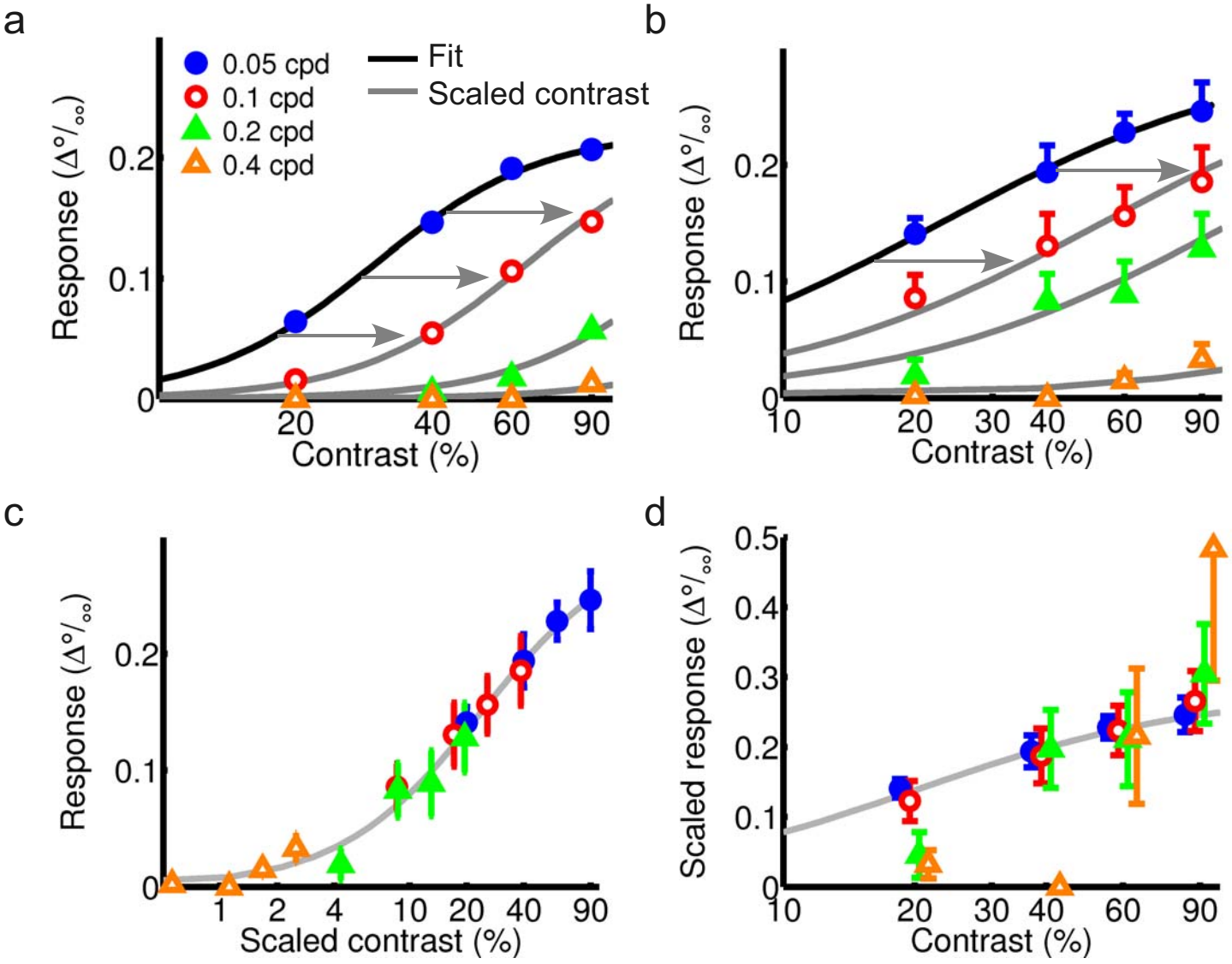
a
0.05 cpd
0.1 cpd
0.2 cpd
0.4 cpd
Fit
Scaled contrast
Response (Δ°/₀₀)
0
0.1
0.2
20
40
60
90
Contrast (%)
b
Response (Δ°/₀₀)
0
0.1
0.2
10
20
30
40
60
90
Contrast (%)
c
Response (Δ°/₀₀)
0
0.1
0.2
1
2
4
10
20
40
90
Scaled contrast (%)
d
Scaled response (Δ°/₀₀)
0
0.1
0.2
0.3
0.4
0.5
10
20
30
40
60
90
Contrast (%)

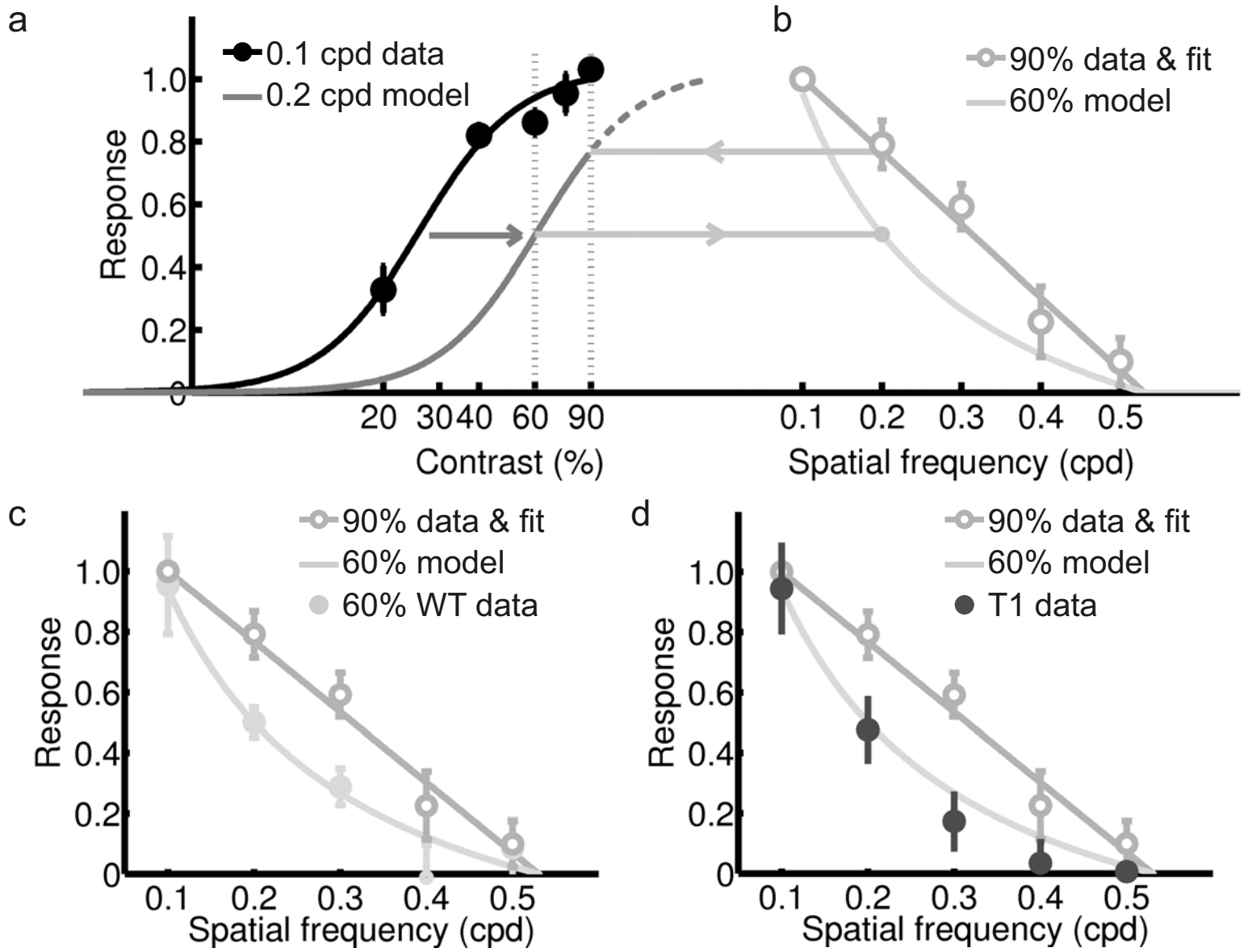
a
0.1 cpd data
0.2 cpd model
Response
1.0
0.8
0.6
0.4
0.2
0
20 30 40 60 90
Contrast (%)
b
90% data & fit
60% model
0.1 0.2 0.3 0.4 0.5
Spatial frequency (cpd)
c
90% data & fit
60% model
60% WT data
Response
1.0
0.8
0.6
0.4
0.2
0
0.1 0.2 0.3 0.4 0.5
Spatial frequency (cpd)
d
90% data & fit
60% model
T1 data
Response
1.0
0.8
0.6
0.4
0.2
0
0.1 0.2 0.3 0.4 0.5
Spatial frequency (cpd)